Computer Physics Communications 224 (2018) 396–404

Contents lists available at ScienceDirect

Computer Physics Communications

journal homepage: www.elsevier.com/locate/cpc

ProbeZT: Simulation of transport coefficients of molecular electronic junctions under environmental effects using Büttiker's probes☆

Roman Korol, Michael Kilgour, Dvira Segal *

Chemical Physics Theory Group, Department of Chemistry, University of Toronto, 80 St. George Street Toronto, Ontario, M5S 3H6, Canada

ARTICLE INFO

Article history:
Received 28 May 2017
Received in revised form 22 September 2017
Accepted 5 October 2017
Available online 13 November 2017

Keywords:
Büttiker probe
Molecular junctions
Transport mechanisms
Thermoelectric efficiency
Thermopower
Onsager coefficients
DNA conductance
Quantum interference

ABSTRACT

We present our in-house quantum transport package, ProbeZT. This program provides linear response coefficients: electrical and electronic thermal conductances, as well as the thermopower of molecular junctions in which electrons interact with the surrounding thermal environment. Calculations are performed based on the Büttiker probe method, which introduces decoherence, energy exchange and dissipation effects phenomenologically using virtual electrode terminals called probes. The program can realize different types of probes, each introducing various environmental effects, including elastic and inelastic scattering of electrons. The molecular system is described by an arbitrary tight-binding Hamiltonian, allowing the study of different geometries beyond simple one-dimensional wires. Applications of the program to study the thermoelectric performance of molecular junctions are illustrated. The program also has a built-in functionality to simulate electron transport in double-stranded DNA molecules based on a tight-binding (ladder) description of the junction.

Program summary
Program Title: ProbeZT
Program Files doi: http://dx.doi.org/10.17632/cvnp3kmcc6.1
Licensing provisions:GPLv3
Programming language: MATLAB
Nature of problem: Quantum transport in molecular electronic systems, covering coherent and incoherent behavior.
Solution method: Implementation of environmental effects using Büttiker probes, resulting in coupled linear equations solved by matrix inversion.
Additional comments including restrictions and unusual features: Voltage and voltage–temperature probe simulations can only be performed in the linear response regime (low voltage bias).

1. Introduction

Studies of charge transport in metal–molecule–metal junctions contribute to fundamental understanding of many-body phenomena at the nanoscale, and to the rational design of molecular electronic devices [1]. Among the molecular elements commonly investigated we recount short saturated and unsaturated organic molecules [2], conducting polymers, biomolecules such as DNA [3,4] and polypeptides [5], single-molecule magnets [6], and self-assembled organic monolayers [7,8]. Beyond the electrical conductance, measurements of the thermopower are useful not only in identifying structures with promising thermoelectric properties, but also in revealing information on charge transport characteristics which may be obfuscated in conductance measurements [9–12].

An intriguing aspect of molecular conductance is the observation of the confluence of different transport mechanisms: quantum coherent, semiclassical, and even fully classical. Specifically, by increasing molecular length, temperature, and by modifying the environment, the electrical conductance manifests the crossover from a fully quantum coherent electronic transmission (deep tunneling or ballistic-resonant quantum transport) to thermally-assisted hopping between localized sites, and even classical diffusion [1], see for example studies on DNA molecules [13,14]. Intermediate quantum coherent–incoherent transport phenomena can also be observed in specific DNA sequences [15,16].

From the theoretical–computational point of view, the crossover between coherent and incoherent transport behavior evinces on

☆ This paper and its associated computer program are available via the Computer Physics Communication homepage on ScienceDirect (http://www.sciencedirect.com/science/journal/00104655).

* Corresponding author.
E-mail addresses: dvira.segal@utoronto.ca, dsegal@chem.utoronto.ca (D. Segal).

https://doi.org/10.1016/j.cpc.2017.10.005
0010-4655/

the interaction of conducting electrons with other degrees of freedom, electrons, nuclei, solvent, local spins, etc. How do we incorporate such many-body effects in transport calculations? The Landauer approach [17], a prominent technique for simulating molecular transport junctions, does not account for incoherent effects, and thus is unsuitable to describe transport in 'flexible' systems. On the other hand, methods which provide a first-principle microscopic description of electron-vibration interactions are computationally expensive, and therefore limited to simulate small systems, see e.g. [18–23].

In recent years the so-called Landauer–Büttiker probe (LBP) technique [24,25] has been applied to address this shortfall and investigate electronic conduction in organic and bio molecular junctions [26–33]. The LBP method was originally introduced to model decoherence effects in mesoscopic systems. It captures many-body scattering effects in a phenomenological manner, by introducing "probes" into the noninteracting Hamiltonian to mimic e.g. incoherent energy exchange processes. Electrons may leave the junction towards the probe, and come back – with a different phase and energy – only conserving the net charge current from the source to the drain.

Using different variants of the LBP method: dephasing probe, voltage and voltage–temperature probes, we demonstrated in a series of papers [34–39] that the LBP technique can provide a meaningful description of molecular electronic conduction under phase loss, inelastic effects, and dissipation: (i) The method captures the tunneling-to-hopping crossover in the electronic conductance and the thermopower [38] by varying e.g. molecular length, fitting to describe conductance in organic molecules [34] and biomolecules [37–39]. (ii) It can provide the current–voltage characteristics at high bias, demonstrating the crucial role of dissipation on the junction's operation [35,36]. (iii) It can describe intermediate coherent–incoherent transport effects [37].

The code presented here has been mainly developed in Refs. [34,35,37–39]. It allows users to calculate electronic transport coefficients in metal–molecule–metal junctions using different flavors of the LBP method, and thus incorporate various types of incoherent effects in transport calculations. Within this package, one specifies a tight-binding Hamiltonian for the molecular junction, or the sequence of a double-stranded (ds) DNA molecule. Other input parameters are the metal-molecule hybridization energy, the temperature of the thermal environment, and the rate constant of environmental effects. Based on that, one receives the electron current and linear response transport coefficients: electrical conductance, electronic thermal conductance, and the Seebeck coefficient, to construct the thermoelectric figure of merit.

The code is written in the MATLAB programming language. Since calculations exemplified here are relatively cheap computationally, there is no need to resort to a coding language optimized for speed. We emphasize the flexibility that this code offers to users looking to simulate complex molecular geometries or nanoelectronic devices. Our hope is that the program would be adapted and included within density-functional theory-nonequilibrium Green's function (DFT-NEGF) simulations of molecular transport coefficients, which to date are in-general performed based on the coherent Landauer formula, see for example Ref. [40].

Various other software packages are dedicated to solving quantum transport problems in the language of the Green's function, yet focusing on other aspects of the problem [41]. In particular, other programs target e.g. extended nanostructures [42] (KWANT), device modeling [43,44] (NEMO5, NEXTNANO), the description of the atomistic structure of the whole system using DFT [45–47] (SMEAGOL, TRANSIESTA, ATOMISTIX TOOLKIT). Nevertheless, incorporating inelastic effects due to electron–nuclei interaction into transport calculations remains a challenge, and is the focus of our software package.

The paper is organized as follows. In Section 2 we present the LBP formalism. In Section 3, we discuss technical details of the code, as well as the handling of inputs and outputs. In Section 4, we describe several examples of how the code can be used to calculate transport properties for linear one-dimensional (1D) chains, DNA sequences, and benzene junctions. In Section 5, we conclude and discuss potential generalizations to the code.

2. Methodology

The physical problem of interest here is of a metal–molecule–metal junction. The Landauer formalism describes quantum coherent transport of particles in the language of transmission functions [17]. To implement incoherent scattering effects of electrons on the junction due to different interactions (electron–electron, electron–nuclei, etc.), we employ the Landauer–Büttiker probe method. The total Hamiltonian reads

$$\hat{H} = \hat{H}_M + \hat{H}_L + \hat{H}_R + \hat{H}_T + \hat{H}_P + \hat{V}_P. \tag{1}$$

The molecular electronic part is described by a tight binding Hamiltonian $\hat{H}_M$ with $n = 1, 2, \ldots, N$ localized sites with energies ϵ_n and inter-site coupling matrix elements $t_{n,m}$,

$$\hat{H}_M = \sum_{n=1}^{N} \epsilon_n \hat{c}_n^\dagger \hat{c}_n + \sum_{n,m=1}^{N-1} t_{n,m} \hat{c}_n^\dagger \hat{c}_m + h.c. \tag{2}$$

Here, $\hat{c}_n^\dagger$ ($\hat{c}_n$) are fermionic creation (annihilation) operators of electrons on each site. The two metal electrodes are modeled by Fermi seas of noninteracting electrons,

$$\hat{H}_\nu = \sum_k \epsilon_{\nu,k} \hat{a}_{\nu,k}^\dagger \hat{a}_{\nu,k}, \quad \nu = L, R, \tag{3}$$

with $\hat{a}_{\nu,k}^\dagger$ ($\hat{a}_{\nu,k}$) as fermionic creation (annihilation) operators of electrons with momentum k in the ν lead. Electrons can tunnel from the L (R) metal to site 1 (N),

$$\hat{H}_T = \sum_k g_{L,k} \hat{a}_{L,k}^\dagger \hat{c}_1 + \sum_k g_{R,k} \hat{a}_{R,k}^\dagger \hat{c}_N + h.c. \tag{4}$$

In the absence of probes, this Hamiltonian dictates phase-coherent electron dynamics. Incoherent scattering effects of electrons on the molecule are introduced by attaching fictitious reservoirs (probes) to the molecule. For simplicity we assume that each electronic site is coupled to an independent probe,

$$\hat{H}_P = \sum_{n=1}^{N} \sum_k \epsilon_{n,k} \hat{a}_{n,k}^\dagger \hat{a}_{n,k}. \tag{5}$$

The nth probe exchanges particles with the nth site of the molecular wire,

$$\hat{V}_P = \sum_{n=1}^{N} \sum_k g_{n,k} \hat{a}_{n,k}^\dagger \hat{c}_n + h.c. \tag{6}$$

Here $\hat{a}_{n,k}^\dagger$ ($\hat{a}_{n,k}$) are fermionic creation (annihilation) operators for an electron in the $n = 1, 2, \ldots, N$-th probe with momentum k and $g_{n,k}$ are the tunneling energies from the nth molecular site into the nth probe. We employ $\nu = L, R$ to identify the (physical) metal electrodes, n to identify the fictitious probe leads, and $\alpha = n, \nu$ to count all metal terminals. Below, we explain the different self consistent conditions which the probes satisfy.

The hybridization energy (broadening) of the molecule to the metal leads, $\gamma_{L,R}$, and its coupling to the probes γ_n is given by

$$\gamma_\alpha(\epsilon) = 2\pi \sum_k |g_{\alpha,k}|^2 \delta(\epsilon - \epsilon_{\alpha,k}). \tag{7}$$

We typically work in the wide-band limit, therefore take γ_α as energy independent parameters. Note that this choice does not pose a central limitation to our code; it is in fact relatively simple to implement different spectral densities for $\gamma_\alpha(\epsilon)$ [34].

It is typical to characterize the interaction with the environment (probes) by a single parameter, $\gamma_p = \gamma_n$. However, site-specific parameters are built-in as an option for our code, and do not in any way affect the implementation. The model (1) does not include explicit many-body interactions, thus the electric current leaving the L contact satisfies the Landauer–Büttiker formula (per spin),

$$I_L = \frac{e}{h}\sum_\alpha \int_{-\infty}^{\infty} \mathcal{T}_{L,\alpha}(\epsilon)\,[f_L(\epsilon) - f_\alpha(\epsilon)]\,d\epsilon. \tag{8}$$

Here, $f_\nu(\epsilon) = [e^{\beta_\nu(\epsilon-\mu_\nu)} + 1]^{-1}$ are the Fermi–Dirac distribution functions in the physical electrodes, given in terms of the temperatures $k_B T_\nu = \beta_\nu^{-1}$ and chemical potentials μ_ν. In contrast, the distribution functions $f_n(\epsilon)$ are determined from the dephasing/voltage/voltage–temperature probe conditions, explained below. In direct analogy to Eq. (8), the net current between the nth probe and the molecular system can be written as

$$I_n = \frac{e}{h}\sum_\alpha \int_{-\infty}^{\infty} \mathcal{T}_{n,\alpha}(\epsilon)\,[f_n(\epsilon) - f_\alpha(\epsilon)]\,d\epsilon. \tag{9}$$

The transmission functions in Eqs. (8) and (9) are obtained from the $(N\times N)$-sized Green's function and the hybridization matrices [48],

$$\mathcal{T}_{\alpha,\alpha'}(\epsilon) = \mathrm{Tr}[\hat{\Gamma}_{\alpha'}(\epsilon)\hat{G}^r(\epsilon)\hat{\Gamma}_\alpha(\epsilon)\hat{G}^a(\epsilon)]. \tag{10}$$

The trace is performed over the N electronic states of the molecule. We assign $\mathcal{T}_{\alpha,\alpha}(\epsilon) = 0$, since these terms do not add to the net current.

The Green's function is defined in terms of the retarded and advanced Green's functions, $\hat{G}^r(\epsilon) = [\epsilon\hat{I} - \hat{H}_M + \frac{i}{2}(\hat{\Gamma}_L + \hat{\Gamma}_R + \sum_n \hat{\Gamma}_n)]^{-1}$, $\hat{G}^a(\epsilon) = [\hat{G}^r(\epsilon)]^\dagger$.

In the code provided and the examples presented here, the molecule is coupled through a single electronic site to the metal leads, thus the hybridization matrices have a single nonzero value,

$$\begin{aligned} &[\hat{\Gamma}_n(\epsilon)]_{n,n} = \gamma_n(\epsilon), \quad n = 1, 2, \ldots, N \\ &[\hat{\Gamma}_L(\epsilon)]_{1,1} = \gamma_L(\epsilon), \quad [\hat{\Gamma}_R(\epsilon)]_{N,N} = \gamma_R(\epsilon), \end{aligned} \tag{11}$$

with the molecule–metal hybridization and the environmental decoherence/dissipation rates $\gamma_\alpha/\hbar$, see Eq. (7). This setup can be easily generalized, to couple the metals to multiple molecular electronic states.

The probe technique can be implemented under different self-consistent conditions, allowing us to craft incoherent electron scattering processes: elastic effects are implemented via the "dephasing probe", dissipative inelastic effects are introduced through the "voltage probe". Inelastic effects can be further studied under the combination of voltage and temperature gradients using the "voltage–temperature probe". As implemented in this code, the dephasing probe can be used at any bias, but the voltage and voltage–temperature probes should be operated only in the linear response regime [49]. Generalizations beyond linear response were discussed in Refs. [35,36], but are not included in the present implementation. Below, we use the following notation for the voltage bias, $\Delta V \equiv \Delta\mu/e$ with $\Delta\mu = (\mu_L - \mu_R)$, and the temperature bias $\Delta T \equiv T_L - T_R$.

2.1. Dephasing probe

Incoherent – but elastic – scattering processes are implemented via the dephasing probe, where we demand *energy resolved* charge conservation: Each probe is required not only to conserve the particle current from the source to the drain, but furthermore, it can neither contribute nor dissipate energy to/from electrons. The dephasing probe can be readily used for calculating the full current–voltage (I–V) characteristics of a molecular junction beyond linear response. More details over the physical action of the dephasing probe are included in Ref. [34].

Input. Based on the molecular electronic parameters, we calculate the transmission functions from Eq. (10). One further needs to supply the Fermi–Dirac distributions $f_{L,R}(\epsilon)$ for the metal electrodes, given in terms of the chemical potentials $\mu_{L,R}$ and temperatures $T_{L,R}$.

Procedure. Mathematically, incoherent-elastic processes are implemented by requiring that the energy resolved charge current to each probe [the integrand in Eq. (9)], nullifies,

$$i_n(\epsilon) = 0, \quad \forall n \tag{12}$$

with the total charge current $I_n = \int i_n(\epsilon)d\epsilon$. Calculations proceed with a two-step procedure:

1. The condition (12) translates into N linear equations for the electron distributions in each probe, $f_n(\epsilon)$. These are received by a matrix inversion at every energy ϵ within the band

   $$\mathbf{M}(\epsilon)\mathbf{f}(\epsilon) = \mathbf{v}(\epsilon). \tag{13}$$

   Here, the unknown probe functions are collected into the vector $\mathbf{f}(\epsilon)$. The inhomogeneous term is

   $$\mathbf{v}_n(\epsilon) = \mathcal{T}_{n,L}(\epsilon)f_L(\epsilon) + \mathcal{T}_{n,R}(\epsilon)f_R(\epsilon). \tag{14}$$

   The $N\times N$ matrix $\mathbf{M}(\epsilon)$ is constructed from the transmission functions,

   $$\mathbf{M}(\epsilon) = \begin{bmatrix} \sum_\alpha \mathcal{T}_{1,\alpha}(\epsilon) & -\mathcal{T}_{1,2}(\epsilon) & -\mathcal{T}_{1,3}(\epsilon) & \ldots \\ -\mathcal{T}_{2,1}(\epsilon) & \sum_\alpha \mathcal{T}_{2,\alpha}(\epsilon) & -\mathcal{T}_{2,3}(\epsilon) & \ldots \\ -\mathcal{T}_{3,1}(\epsilon) & -\mathcal{T}_{3,2}(\epsilon) & \sum_\alpha \mathcal{T}_{3,\alpha}(\epsilon) & \ldots \\ \ldots & \ldots & \ldots & \ldots \end{bmatrix}$$

   Note that the distribution functions $f_n(\epsilon)$ do not necessarily follow the Fermi–Dirac functional form, though they are typically close to that in linear response [36]. Eq. (13) is solved for a fine grid of energies ϵ, to receive the distributions $f_n(\epsilon)$.
2. Given charge conservation (based on the probe condition), the net source (L) to drain (R) electric current across the junction is calculated from Eq. (8), by summing up all the currents leaving the left terminal.

Output. The dephasing probe provides the current–voltage characteristics even beyond linear response. For example, assuming $T_L = T_R$, we simulate I as a function of bias voltage $\Delta\mu$, or depict the conductance $G \equiv I/\Delta V$.

2.2. Voltage probe $\Delta\mu \neq 0$, $\Delta T = 0$.

The voltage probe is used to study the electrical conductance of molecular junctions in the linear response regime, $\Delta\mu = \mu_L - \mu_R \ll T, \gamma_\alpha$. This probe allows for incoherent-inelastic effects, potentially with heat absorption/release on the junction. We consider here a junction with a fixed temperature all through. One could generalize this setup and describe the electrical conductance of a dissipative junction under a temperature gradient.

Input. Based on the molecular electronic parameters, we evaluate the transmission functions from Eq. (10). One further needs to provide the applied bias voltage $\Delta\mu = \mu_L - \mu_R$ and the temperature $T = T_\alpha$.

Procedure. Incoherent inelastic-dissipative effects can be introduced by requiring the net *total* particle current flowing between each probe and the system, Eq. (9), to vanish, while allowing energy exchange,

$$I_n = \frac{e}{h}\sum_{\alpha}\int_{-\infty}^{\infty}\mathcal{T}_{n,\alpha}(\epsilon)\left[f_n(\epsilon)-f_\alpha(\epsilon)\right]d\epsilon = 0, \quad \forall n. \tag{15}$$

We require the probe distribution functions to take the form of Fermi–Dirac functions, $f_n(\epsilon) = [e^{\beta(\epsilon-\mu_n)}+1]^{-1}$. In principle, solving for μ_n is a nonlinear problem, which can be numerically addressed as was discussed in e.g. Refs. [35,36]. In the current implementation, however, we restrict our calculations to the linear response regime. Assuming low voltage, we Taylor-expand the Fermi–Dirac functions to first-nontrivial order,

$$f_\alpha(\epsilon,\mu_\alpha) = f_{eq}(\epsilon,\epsilon_F) - \frac{\partial f_{eq}(\epsilon,\epsilon_F)}{\partial\epsilon}(\mu_\alpha-\epsilon_F). \tag{16}$$

We explicitly indicate the dependency of the Fermi function on the Fermi energy $\epsilon_F = \mu_{eq}$. For convenience, below we set $\epsilon_F = 0$. In linear response, Eq. (15) reduces into a set of N linear equations,

$$\begin{aligned}&\mu_n\sum_{\alpha}\int_{-\infty}^{\infty}\left(-\frac{\partial f_{eq}}{\partial\epsilon}\right)\mathcal{T}_{n,\alpha}(\epsilon)d\epsilon\\ &-\sum_{n'=1}^{N}\mu_{n'}\int_{-\infty}^{\infty}\left(-\frac{\partial f_{eq}}{\partial\epsilon}\right)\mathcal{T}_{n,n'}(\epsilon)d\epsilon\\ &=\int_{-\infty}^{\infty}d\epsilon\left(-\frac{\partial f_{eq}}{\partial\epsilon}\right)\left[\mathcal{T}_{n,L}(\epsilon)\mu_L+\mathcal{T}_{n,R}(\epsilon)\mu_R\right].\end{aligned} \tag{17}$$

We proceed with a two-step procedure:

1. The N equations above can be recast into $\boldsymbol{M}\boldsymbol{\mu} = \mathbf{v}$, to be solved by a single matrix inversion and provide the chemical potentials of the probes at each site, μ_n.
2. We calculate the net charge current flowing across the system in linear response by linearizing Eq. (8), using the probes' chemical potentials,

$$I = \frac{e}{h}\sum_{\alpha}\left[\int_{-\infty}^{\infty}\mathcal{T}_{L,\alpha}(\epsilon)\left(-\frac{\partial f_{eq}}{\partial\epsilon}\right)d\epsilon\right](\mu_L-\mu_\alpha). \tag{18}$$

Output. The voltage probe method yield the linear-response electrical conductance of the junction, $G \equiv I/\Delta V$.

2.3. Voltage–Temperature probe, $\Delta\mu \neq 0$, $\Delta T \neq 0$

This probe adds an energy conservation condition to the previously described voltage probe. It implements thus incoherent-inelastic—yet non-dissipative scattering effects. As such, it can be used to calculate Onsager coefficients for two-terminal (source–drain) thermoelectric transport, in the presence of incoherent effects.

Input. Based on the molecular electronic parameters, we calculate all transmission functions from Eq. (10). We further provide parameters for the physical metal electrodes: the chemical potentials $\mu_{L,R}$ and temperatures $T_{L,R}$.

Procedure. The potential and temperature profiles for the probes are calculated from two sets of conditions, for charge conservation and zero heat dissipation on the junction ($n = 1, 2, \ldots, N$),

$$\begin{aligned}I_n &= \frac{e}{h}\sum_{\alpha}\int_{-\infty}^{\infty}d\epsilon\mathcal{T}_{n,\alpha}(\epsilon)\left[f_n(\epsilon)-f_\alpha(\epsilon)\right] = 0,\\ Q_n &= \frac{1}{h}\sum_{\alpha}\int_{-\infty}^{\infty}d\epsilon(\epsilon-\mu_n)\mathcal{T}_{n,\alpha}(\epsilon)\left[f_n(\epsilon)-f_\alpha(\epsilon)\right] = 0.\end{aligned} \tag{19}$$

These two requirements translate into $2\times N$ non-linear equations for μ_n and T_n, to provide nonlinear transport coefficients. Here, we are only concerned with linear response coefficients, thus we Taylor-expand the Fermi–Dirac functions around the equilibrium temperature $T_{eq} = (T_L+T_R)/2$ and chemical potential $\epsilon_F = (\mu_L+\mu_R)/2$,

$$\begin{aligned}&f_\alpha(\epsilon,T_\alpha,\mu_\alpha) = f_{eq}(\epsilon,T_{eq},\epsilon_F)\\ &-\frac{\partial f_{eq}(\epsilon,T_{eq},\epsilon_F)}{\partial\epsilon}\left[\frac{\epsilon-\epsilon_F}{T_{eq}}(T_\alpha-T_{eq})+(\mu_\alpha-\epsilon_F)\right].\end{aligned} \tag{20}$$

The derivatives are evaluated at the Fermi energy ϵ_F, taken as the reference point in our calculations. Under the linear approximation, Eq. (19) reduces to ($p = 0, 1$),

$$\begin{aligned}&\sum_{\alpha}\int_{-\infty}^{\infty}d\epsilon\mathcal{T}_{n,\alpha}(\epsilon)\left(-\frac{\partial f_{eq}}{\partial\epsilon}\right)(\epsilon-\epsilon_F)^p\\ &\times\left[\frac{\epsilon-\epsilon_F}{T_{eq}}(T_n-T_\alpha)+(\mu_n-\mu_\alpha)\right] = 0.\end{aligned} \tag{21}$$

The N equations with $p = 0$ ($p = 1$) correspond to charge (heat) current conservation equations (19). We proceed as follows:

1. Eq. (21) organizes into a linear set, $\boldsymbol{M}\boldsymbol{\lambda} = \mathbf{v}$, with $\mathbf{M}$ comprising the $2N$ equations as explained above, $\boldsymbol{\lambda}$ a vector listing the probe temperatures and chemical potentials, and $\mathbf{v}$ the inhomogeneous term in Eq. (21), organized from expressions involving $T_{L,R}$ and $\mu_{L,R}$. We solve this linear system by a matrix inversion and obtain the probes' chemical potentials μ_n and temperatures T_n.
2. Linearizing Eq. (8), we receive

$$\begin{aligned}I &= \frac{e}{h}\sum_{\alpha}\left[(\mu_L-\mu_\alpha)\int_{-\infty}^{\infty}\mathcal{T}_{L,\alpha}(\epsilon)\left(-\frac{\partial f_{eq}}{\partial\epsilon}\right)d\epsilon\right.\\ &\left.+\,(T_L-T_\alpha)\int_{-\infty}^{\infty}\mathcal{T}_{L,\alpha}(\epsilon)\left(-\frac{\partial f_{eq}}{\partial\epsilon}\right)\left(\frac{\epsilon-\epsilon_F}{T_{eq}}\right)d\epsilon\right].\end{aligned} \tag{22}$$

Similarly, the heat current, evaluated at the left contact is received as follows,

$$\begin{aligned}Q &= \frac{1}{h}\sum_{\alpha}\left[(\mu_L-\mu_\alpha)\int_{-\infty}^{\infty}(\epsilon-\mu_L)\mathcal{T}_{L,\alpha}(\epsilon)\left(-\frac{\partial f_{eq}}{\partial\epsilon}\right)d\epsilon\right.\\ &+\,(T_L-T_\alpha)\\ &\left.\times\int_{-\infty}^{\infty}(\epsilon-\mu_L)\mathcal{T}_{L,\alpha}(\epsilon)\left(-\frac{\partial f_{eq}}{\partial\epsilon}\right)\left(\frac{\epsilon-\epsilon_F}{T_{eq}}\right)d\epsilon\right].\end{aligned} \tag{23}$$

Output. Using this procedure, we can extract the junction's electrical conductance, thermopower, and the electronic thermal conductance, then calculate the thermoelectric figure of merit ZT. First, we note that in the linear response regime, the electric and heat currents can be formally written as [50]

$$I = G\Delta V + GS\Delta T, \tag{24}$$

$$Q = G\Pi\Delta V + (K+GS\Pi)\Delta T. \tag{25}$$

The thermopower S, or the Seebeck coefficient, is defined as

$$S \equiv -\frac{\Delta V}{\Delta T}\Big|_{I=0}. \tag{26}$$

In the linear response regime the maximum thermoelectric efficiency, of heat to work conversion, is related to Carnot efficiency $\eta_C = 1-T_C/T_H$ by [50]

$$\eta_{max} = \eta_C\frac{\sqrt{ZT+1}-1}{\sqrt{ZT+1}+1}, \tag{27}$$

with the thermoelectric figure of merit

$$ZT = \frac{GS^2}{K}T. \tag{28}$$

We employ the voltage–temperature procedure twice. First, we apply a voltage bias $\Delta V \neq 0$, but assume that $\Delta T = 0$. Based on the linearized currents, Eq. (24), we extract G and Π. Next, we apply a temperature difference $T_L > T_R$ at zero voltage bias. From this calculation, and using the values for G and Π, we evaluate the thermopower S and the electronic thermal conductance K. Combining these coefficients we receive ZT.

3. Technical details

3.1. Program structure

We provide two packages. `Linear-DNA` and `GeneralHamiltonian`. The `Linear-DNA` package simulates linear, N-site molecules: 1-dimensional chains or double-stranded (ds) DNA sequences. It can be immediately applied to study transport properties as a function of molecular length. The `GeneralHamiltonian` package adds great flexibility: It allows one to define an arbitrarily complex tight-binding Hamiltonian, distinct probe couplings at each site, and to choose which molecular states interact with the probes. Overall, the two packages run an identical algorithm, and are structurally similar. Further, as much as possible we maintain identical parameters and variable names between the two packages.

All energy variables are given in units of eV. Temperature is inputted in Kelvin. Since we do not include the prefactor e^2/h in our code when calculating the electrical conductance G, it is received directly in units of the quantum of conductance, $G_0 = e^2/h$.

Similarly, since the factors k_B and e are missing in the calculation of the thermopower S, it is directly computed in units of (k_B/e). The electronic thermal conductance K requires more attention. It is provided in our program in units of eV. To convert it to its physical units, one needs to multiply it by the (missing) factor $(e \times k_B/h)$ in MKS, which converts it to J/(K sec). It can be also meaningfully presented via the Wiedemann–Franz law, by displaying the dimensionless ratio $K/(TGL)$ with $L \equiv \pi^2 k_B^2/3e^2$. The figure of merit ZT is output as a dimensionless coefficient.

The simulation script for the program is `main.m`. It contains the backbone of the algorithm: it reads data, loops over different parameters, and manages outputs. The overall algorithm goes as follows:

1. The script `Input.m` initializes parameters and the conditions under which the system is simulated. In the `Linear-DNA` package, the choice (`calctype=1`) initializes the linear 1-dimensional model, by setting the parameters of the molecular electronic Hamiltonian $\hat{H}_M$: molecular length, site energies ϵ_n, and tunneling terms $t_{n,m}$. Energy parameters are all given in units of eV. For the ds-DNA model (`calctype=2`), the DNA sequences studied are directly specified instead. One should enter the sequences along a single strand, from the 5' to the 3' end. The metal leads are connected to the 3' sites [51]. In the `GeneralHamiltonian` package, the initialization process includes the construction of the studied Hamiltonians and hybridization matrices, thus this package does not include a separate `hamiltonian.m` function. One should select the type of the probe (`probe=1, 2, 3` for dephasing, voltage, or voltage–temperature probe, respectively), the temperature, metal-molecule hybridization energies $\gamma_{L,R}$, and molecule-probe interaction energy γ_p. The metallic bands are assumed to extend between $\pm D$, taken as a large parameter (5 eV in our simulations). Numerical integration is performed by a simple quadrature summation over a fine grid. The default setting is $d\epsilon \sim 10^{-3}$ eV, though the mesh size should always be smaller than the smallest (physical) energy parameter of the system.
2. The script `definitions.m` lists physical constants used in the computation: the Fermi energy $\epsilon_F = 0$, the applied source–drain voltage bias. It also generates the energy grid for numerical integration based on D, $d\epsilon$, entered in `Input.m`, as well as the matrices for keeping the output data.
3. The functions `hamiltonianLinear.m` and `hamiltonianDNA.m` build the Hamiltonian matrix $\hat{H}_M$ for a linear chain or the DNA model, based on the parameters specified in the script `Input.m`. The `hamiltonianLinear.m` function can be easily modified to model more complex models, beyond a linear chain. In fact, besides the built-in construction of site 1 and N attached to the L and R leads, respectively, the system Hamiltonian can be adapted to an arbitrary tight-binding network.
4. The function `transmission.m` computes the energy dependent transmission functions between every pair of terminals $\mathcal{T}_{\alpha,\alpha'}(\epsilon)$. If the probes are inactive ($\gamma_p = 0$), this calculation is performed in a trivial way, producing zero transmission functions for processes involving probes. Note that for the setups considered in this code, the transmission functions are always symmetric, $\mathcal{T}_{\alpha,\alpha'}(\epsilon) = \mathcal{T}_{\alpha',\alpha}(\epsilon)$.
5. The functions `dprobe.m`, `vprobe.m`, `vtprobe.m` construct the relevant matrix $\mathbf{M}$, and solve the appropriate set of linear equations, as described in Sections 2.3, 2.1 and 2.2, for the dephasing, voltage and voltage–temperature probe, respectively. In the `Linear-DNA` package, the conductance is the only output of the dephasing and voltage probes. In the `GeneralHamiltonian` package, the dephasing probe can be used to simulate the I–V characteristics at high bias. The voltage–temperature probe provides the thermoelectric linear response coefficients: conductance, thermopower, thermal conductance and the figure of merit.
6. Results are saved as `dataD.mat`, `dataV.mat` or `dataVT.mat`, when using the dephasing, voltage, or voltage–temperature probes, respectively.

3.2. Package details

`Linear-DNA` package

- `main.m`
- `Input.m`
- `definitions.m`
- `hamiltonianLinear.m`
- `hamiltonianDNA.m`
- `transmission.m`
- `dprobe.m`
- `vprobe.m`
- `vtprobe.m`

`GeneralHamiltonian` package

- `main_general.m`
- `Input_general.m`
- `definitions_general.m`
- `transmission_general.m`
- `dprobe.m`
- `vprobe.m`
- `vtprobe.m`

4. Examples

In this section, we present some results from the ProbeZT package. First, we describe the application of the `Linear-DNA`

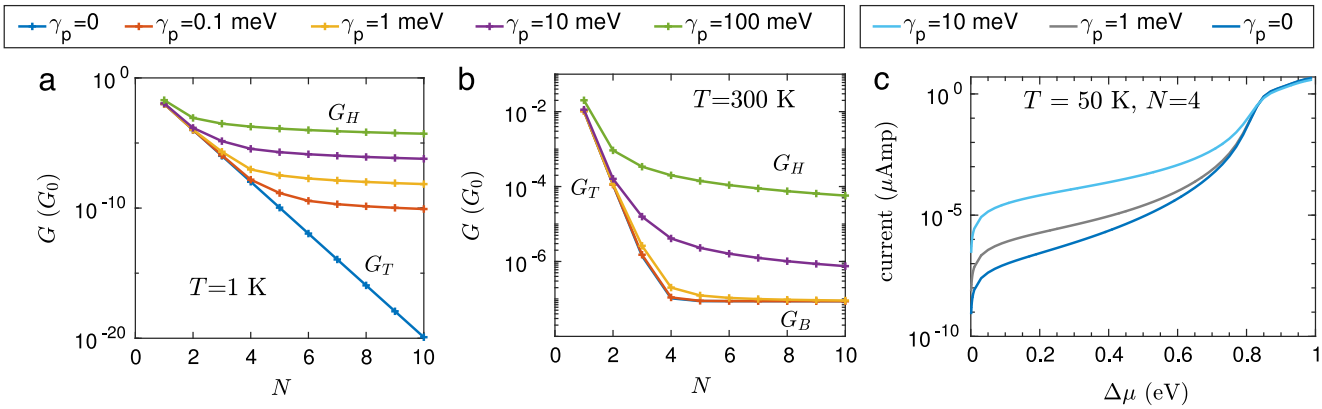

Fig. 1. (a)–(b) Electrical conductance of a uniform 1D molecular chain with $\epsilon_B = 0.5$ eV, $t_{n,n\pm1} = 50$ meV, $\gamma_{L,R} = 50$ meV, $\Delta\mu = 10$ meV. Computations were performed using the dephasing probe. (c) I–V characteristics for one of the chains in (a)–(b) with length $N = 4$ at temperature $T = 50$ K. For simplicity, the molecular parameters are kept fixed under bias.

code to simulate the thermoelectric performance of 1D chains and ds-DNA molecules. We then exercise the `GeneralHamiltonian` program, and study quantum interference and decoherence in a single benzene molecular junction with a meta connection to the metal leads.

4.1. Linear 1D chains: current, conductance, thermoelectric performance

Fig. 1 displays representative conductance and current results for linear molecular wires representing e.g. conjugated polymers [8]. Simulations were performed using the dephasing probe (`probe=1` in `Input.m`). The chain is uniform: the molecular sites take the same energy ϵ_B, and nearest-neighbor coupling is described by a single tunneling element t. The chain is coupled to the leads via the hybridization energies $\gamma_{L,R}$, and to the probe terminals by the energy γ_p. The Hamiltonian of this system is generated automatically by our code by setting `calctype=1` and providing the desired system and environmental parameters in `Input.m`.

The probe technique introduces incoherent effects into the transport behavior, on top of coherent phenomena. Panels (a)–(b) in Fig. 1 clearly demonstrate the contribution of different transport mechanisms to molecular conduction: deep tunneling G_T at low temperatures and for short chains, resonant-coherent (ballistic) conduction G_B at high temperatures and for long chains weakly coupled to the probes, and multi-step hopping G_H for long chains at high γ_p. The dephasing probe can be further employed to study the I–V characteristics of the junction under high voltage bias, see panel (c). This option is only included in the `GeneralHamiltonian` package; It provides the conductance $I/\Delta V$ at high bias, allowing one to recover the current itself.

Using the voltage–temperature probe (`probe=3` in `Input.m`), we analyze the junction's performance as a thermoelectric device. The program computes the junction's electrical conductance, Seebeck coefficient, electronic thermal conductance, and ZT figure of merit. An example is displayed in Fig. 2, using a uniform wire (identical to the last example) with $\epsilon_B = 0.5$ eV and $t = 0.05$ eV. Panel (a) demonstrates the tunneling-to-hopping crossover of the conductance in this off-resonant case. Panel (b) shows the corresponding subtle trend in the thermopower: It increases linearly in the deep tunneling regime, saturates in the hopping regime, but shows high values for small γ_p, when resonant conduction dominates [38]. The thermopower is given in units of k_B/e. Thus, using the electron charge (with its negative sign), we receive negative values for S in the present model, consistent with the fact that transport here takes place via the LUMO of the junction ($\epsilon_B > \epsilon_F$). In panel (c), we further test the Wiedemann–Franz (WF) law [50]. For coherent conduction, when the transmission function does not show significant features around the Fermi energy (in other words, when the Seebeck coefficient is very small), the Wiedemann–Franz law should be satisfied, $K/(TGL) = 1$ with $L \equiv \pi^2 k_B^2/(3e^2)$. We find that the WF law is approximately satisfied in the hopping regime, but when γ_p is small, large deviations appear, in accord with the behavior of S in panel (b). The thermoelectric figure of merit in panel (d) shows a non-monotonic behavior, indicating that short chains of $N = 3$ sites, with weak environmental effects, could be advantageous for thermoelectric applications.

4.2. ds-DNA Junctions

In recent studies, we simulated the conductance and the thermopower of ds-DNA molecules, observing the tunneling to hopping crossover as a function of the barrier width, i.e., the number of A:T base pairs at the center of the sequence [38,39]. Here, A, G, C and T are the adenine, guanine, cytosine and thymine bases, respectively. The package `Linear-DNA` with `calctype` = 2 can be used to generate such results, as well as the electronic thermal conductance and the thermoelectric figure of merit.

We model the electronic structure of ds-DNA molecules with a tight-binding Hamiltonian, which is described in detail in Refs. [37,52,53]. Here we only note that the parametrization, developed in Ref. [52], captures the double-helical topology of ds-DNA as well as its chirality. We simplify this parametrization, and assign a single averaged value for the site energies of the different DNA bases, by following Ref. [53].

The Hamiltonian for the ds-DNA is constructed automatically in `hamiltonianDNA.m` from a base pair sequence defined in `Input.m`. The sequences are inputted as a cell array of 5' to 3' ordered strings with letters 'a', 'c', 'g', 't' standing for the corresponding nucleotide in the sequence. For example, the ds-DNA molecules 5'-ACGC$(AT)_m$GCGT-3' and 5'-ACGC$(AT)_{m-1}$AGCGT-3', $m = 1 - 4$, with 9 to 16 base pairs, are prepared by defining `sequence_cell = {'acgcagcgt', 'acgcatgcgt', 'acgcatagcgt', 'acgcatatgcgt', 'acgcatatagcgt', 'acgcatatatgcgt', 'acgcatatatatgcgt'}`. The molecule is connected to the two leads through the 3' sites. Similarly to the previous examples, one needs to specify the metal-molecule hybridization energy $\gamma_{L,R}$, and the electron-environment interaction energy, encapsulated within the parameter γ_p. For simplicity, we used a single value γ_p, identical for all bases. Further, the position of the Fermi energy is defined in `hamiltonianDNA.m`, and it is given by the variable `EFermi`. It is set in the present simulations to the energy of the G base.

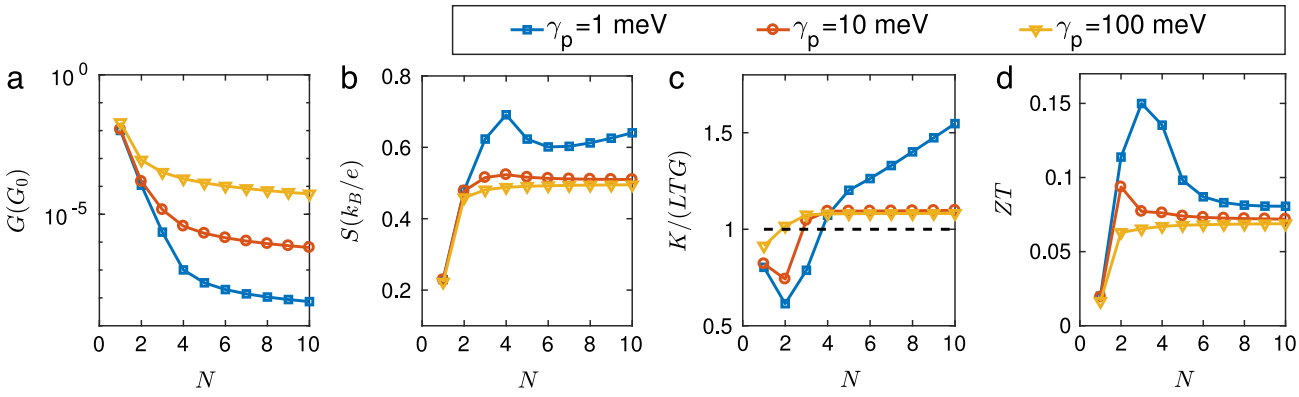

Fig. 2. Linear response transport coefficients of a uniform 1D chain at $T = 200$ K, with the same parameters as in Fig. 1. Simulations were performed using the voltage–temperature probe.

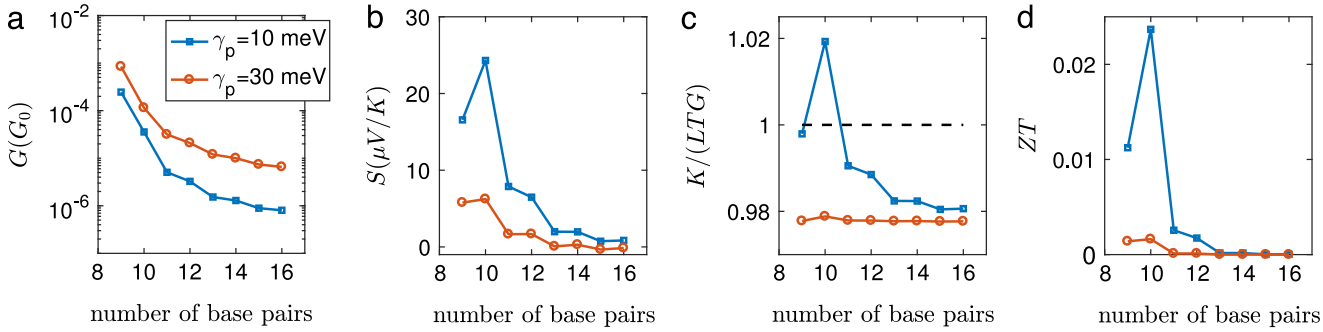

Fig. 3. Linear transport coefficients of ds-DNA molecules with an increasingly long A:T segment. (a) Conductance, (b) thermopower, (c) electronic thermal conductance, and (d) thermoelectric figure of merit. Sequences are ACGC(AT)$_m$GCGT and ACGC(AT)$_{m-1}$AGCGT ($m = 1 - 4$), see Ref. [38]. Simulations were performed at $T = 5$ K to attenuate the contribution of ballistic electrons. Other parameters are $\gamma_p = 10$ and 30 meV, $\gamma_{L,R} = 50$ meV.

Fig. 3 displays simulation results for ds-DNA sequences with an A:T barrier using the voltage–temperature probe, setting `probe=3` in `Input.m`. These sequences were examined experimentally in Ref. [14] and modeled in great detail in our recent work [38]. Our simulations reproduce qualitatively the measurements, displaying the crossover from tunneling to hopping conduction upon the increase of the number of A:T base pairs. In addition to the conductance and the thermopower, which were studied in Ref. [38], we present here the electronic thermal conductance and the thermoelectric figure of merit ZT for DNA. We find that these sequences obey the Wiedemann–Franz law. The attained ZT values are therefore quite small, though again we note that short (but not ultra-short) molecules could be optimized for thermoelectric applications.

An important caveat of our simulations is the promotion of ballistic transport beyond what one expect in reality for DNA molecules. This is because the underlying electronic structure used here is static, and dynamical-nuclear effects are missing. To minimize the contribution of resonant conduction, we reduce the temperature—while keeping environmental effects active with a finite γ_p. For more details, see Ref. [38]. To circumvent this pitfall, it would be useful to perform probe simulations on a large ensemble of configurations generated from e.g. classical molecular dynamic simulations [54,55].

4.3. Quantum interference in benzene junctions

Manifestations of quantum interference effects in molecular electronic junctions have captured much attention in recent years, see for example Refs. [56–58]. We exemplify here the application of the `GeneralHamiltonian` code to study the impact of environmental interactions on quantum interference in benzene nanojunctions. It is known that when a benzene molecule is attached in a meta configuration to two metal leads, electrons passing through it suffer destructive interference, resulting in a low conductance near the Fermi energy, relative to the para configuration. For a recent study, see Ref. [57].

The tight-binding Hamiltonian of the benzene junction is constructed within the `Input_general.m` script as

$$\mathbf{hh} = \begin{bmatrix} 0 & \mathtt{tn} & 0 & 0 & 0 & \mathtt{tn} \\ \mathtt{tn} & 0 & \mathtt{tn} & 0 & 0 & 0 \\ 0 & \mathtt{tn} & 0 & \mathtt{tn} & 0 & 0 \\ 0 & 0 & \mathtt{tn} & 0 & \mathtt{tn} & 0 \\ 0 & 0 & 0 & \mathtt{tn} & 0 & \mathtt{tn} \\ \mathtt{tn} & 0 & 0 & 0 & \mathtt{tn} & 0 \end{bmatrix} \tag{29}$$

The variable `tn` stands for the tight-binding parameter t in the code.

We further set $\epsilon_B = 0$ and $t = 2$ eV, taken from e.g. Ref. [28]. The script `Input_general.m` allows to use distinct probe couplings on each site. Here we introduce a single probe on site 2, 3, 4, or 6 with $\gamma_p = 2$ eV, see Fig. 4. The choice `LeadsL=[1]; LeadsR=[5];` places the metal leads in a meta configuration. We employ the voltage probe to introduce incoherent effects, defined by setting `probe=2`. In Fig. 4, we study the effect of a single, strongly coupled voltage probe, attached to an atom in the ring, on the direct left-to-right transmission function $\mathcal{T}_{L,R}(\epsilon)$. Under environmental interactions, this component suffers decoherence effects. However, bath-assisted contributions (responsible for the development of an ohmic conduction) are missing from the direct transmission $\mathcal{T}_{L,R}(\epsilon)$. In panel (a), we show the case with no probes, and observe a series of anti-resonances resulting from quantum interference in the molecule. By attaching a probe to site 2 or 4, which are exactly equivalent given the symmetric nature of the system at low bias, we observe that the destructive interference at the Fermi

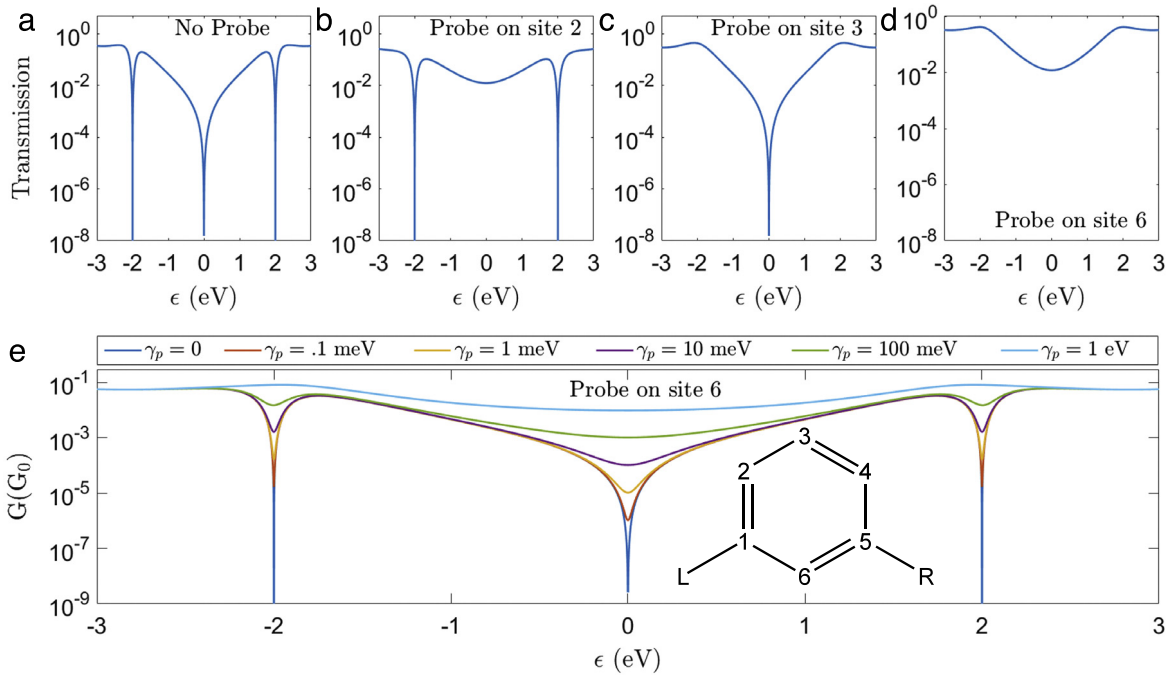

Fig. 4. Interference and decoherence in benzene junctions. (a)–(d) Left-to-right transmission function $\mathcal{T}_{L,R}(\epsilon)$ for a 6-member meta-connected ring with $\epsilon_B = 0$, $t = 2$ eV, $\gamma_{L,R} = 2$ eV and (a) $\gamma_p = 0$, (b), (c) and (d), $\gamma_p = 2$ eV, with a single probe attached to sites 2, 3 and 6 respectively. (e) Low-bias conductance as a function of the Fermi energy, for $T = 5$ K. Inset: benzene ring attached to two metal leads in a meta configuration, with numbered carbons for reference. Here 'L' and 'R' identify the metal contacts.

energy is damped (panel (b)). In panel (c), we attach a probe to site 3, and find that this choice leaves the anti-resonance at the Fermi energy untouched, though anti-resonances in the wings of the transmission function are destroyed. In panel (d), we find that a probe placed on site 6 destroys every anti-resonance in the transmission function. We further show in panel (e) the effect of the probe on the conductance, scanned over the position of the Fermi function.

We find that the anti-resonances are extremely fragile to incoherent effects as introduced by a probe, and they significantly dampen out as we increase γ_p.

How do we receive the transmission and conductance as a function of energy, Fig. 4, within our package? Consider Eq. (8) at low temperature and voltage bias. The difference of Fermi functions reduces to a Dirac delta function and one gets,

$$I_L = \sum_{\alpha} \mathcal{T}_{L,\alpha}(\epsilon_F)(\mu_L - \mu_\alpha), \tag{30}$$

or the conductance $G = \mathcal{T}_{L,R}(\epsilon_F) + \sum_{\nu} \mathcal{T}_{L,\nu}(\epsilon_F)(\mu_L - \mu_\nu)/\Delta\mu$. Since we are calculating all transmission functions, we can readily compute the behavior of the conductance as a function of energy. This option in included in our package as an example, using the `vprobe_trans.m` script instead of `vprobe.m`.

5. Summary

We have presented a software package, `ProbeZT`, for computing the electrical conductance and thermoelectric properties of molecular electronic junctions. The method simulates incoherent effects (decoherence, inelastic effects, dissipation) on the junction by implementing the Büttiker probe method into the Landauer formalism. Our code allows users to simulate uniform 1D or ds-DNA systems via built-in programs, or arbitrary tight-binding geometries using user-defined parameters. Future extensions include the simulation of junctions in which the electrodes hybridize with multiple atoms [59].

The code is relatively short. The current implementation is efficient for systems with $N < 15$ sites. Other parameters that critically determine runtime are the metallic bandwidth D and its energy discretization. We recommend users to work with $D < 10$ eV and $d\epsilon > 10^{-4}$ eV for systems of 1 meV$\leq \epsilon_B, t, \gamma_{p,L,R}, k_BT \leq 1$ eV. Advanced MATLAB users will find it easy to modify and extend the code to study more involved applications, for example two-dimensional systems.

Our hope is that this software would encourage the implementation of Büttiker's probes into DFT-NEGF calculations of nanoelectronic systems [46]. Particularly, with growing experimental capabilities in measuring single-molecule DNA conduction, see for example [13–15,32,33,60], we expect this package to assist in identifying sequences of desired electronic and thermal properties.

Acknowledgments

The work was supported by the Natural Sciences and Engineering Research Council of Canada and the Canada Research Chair Program. The work of Michael Kilgour was partially funded by an Ontario Graduate Scholarship. Roman Korol was funded by the University of Toronto Excellence Research Fund and by the CQIQC at the University of Toronto.

References

[1] J.C. Cuevas, E. Scheer, Molecular Electronics: An Introduction to Theory and Experiment, World Scientific Publishing Company, Singapore, 2010.
[2] T.A. Su, M. Neupane, M.L. Steigerwald, L. Venkataraman, C. Nuckolls, Nature Rev. Mater. 1 (2016) 16002.
[3] S.O. Kelley, J.K. Barton, Science 283 (1999) 375–381.
[4] N.B. Muren, E.D. Olmon, J.Q. Barton, Phys. Chem. Chem. Phys. 14 (2012) 13754–13771.
[5] N. Amdursky, D. Marchak, L. Sepunaru, I. Pecht, M. Sheves, D. Cahen, Adv. Mater. 26 (2015) 7142–7161.
[6] A.C. Aragones, D. Aravena, J.I. Cerda, Z. Acis-Castillo, H. Li, J.A. Real, F. Sanz, J. Hihath, E. Ruiz, I. Diez-Perez, Nano Lett. 16 (2016) 218–226.
[7] C.A. Nijhuis, W.F. Reus, G.M. Whitesides, J. Am. Chem. Soc. 131 (2009) 17814–17827.
[8] S.H. Choi, B. Kim, C.D. Frisbie, Science 320 (2008) 1482–1486.

[9] J.A. Malen, S.K. Yee, A. Majumdar, R.A. Segalman, Chem. Phys. Lett. 491 (2010) 109–122.
[10] L. Rincon-Gracia, C. Evangeli, G. Rubio-Bollinger, N. Agrait, Chem. Soc. Rev. 45 (2016) 4285–4306.
[11] L. Cui, R. Miao, C. Jiang, E. Meyhofer, P. Reddy, J. Chem. Phys. 146 (2017) 092201.
[12] J.R. Widawsky, P. Darancet, J.B. Neaton, L. Venkataraman, Nano Lett. 12 (2012) 354–358.
[13] T. Hines, I. Diez-Perez, J. Hihath, H. Liu, Z.-S. Wang, J. Zhao, G. Zhou, K. Müllen, N. Tao, J. Am. Chem. Soc. 132 (2010) 11658–11664.
[14] Y. Li, L. Xiang, J. Palma, Y. Asai, N. Tao, Nature Commun. (2016) 11294.
[15] L. Xiang, J.L. Palma, C. Bruot, V. Mujica, M.A. Ratner, N. Tao, Nature Chem. 7 (2015) 221–226.
[16] C. Liu, L. Xiang, Y. Zhang, P. Zhang, D.N. Beratan, Y. Li, N. Tao, Nature Chem. 8 (2016) 941–945.
[17] R. Landauer, IBM J. Res. Dev. 1 (1957) 223–231.
[18] A. Mitra, I. Aleiner, A.J. Millis, Phys. Rev. B 69 (2004) 245302.
[19] F. Haupt, M. Leijnse, H.L. Calvo, L. Classen, J. Splettstoesser, M.R. Wegewijs, Phys. Status Solidi b 250 (2013) 2315–2329.
[20] M. Galperin, M.A. Ratner, A. Nitzan, J. Phys.: Condens. Matter 19 (2007) 103201.
[21] R. Hützen, S. Weiss, M. Thorwart, R. Egger, Phys. Rev. B 85 (2012) 121408.
[22] L. Simine, D. Segal, J. Chem. Phys. 138 (2013) 214111.
[23] E.Y. Wilner, H. Wang, M. Thoss, E. Rabani, Phys. Rev. B 89 (2014) 205129.
[24] M. Büttiker, Phys. Rev. B 32 (1985) 1846.
[25] M. Büttiker, Phys. Rev. B 33 (1986) 3020.
[26] D. Nozaki, Y. Girard, K. Yoshizawa, J. Phys. Chem. C 112 (2008) 17408–17415.
[27] D. Nozaki, C. Gomes da Rocha, H.M. Pastawski, G. Cuniberti, Phys. Rev. B 85 (2012) 155327.
[28] S. Chen, Y. Zhang, S. Koo, H. Tian, C. Yam, G. Chen, M. Ratner, J. Phys. Chem. Lett. 5 (2014) 2728–2752.
[29] R. Venkataramani, E. Wierzbinski, D.H. Waldeck, D.N. Beratan, Faraday Discuss. 174 (2014) 57–78.
[30] A.-M. Guo, Q.-F. Sun, Phys. Rev. Lett. 108 (2012) 218102.
[31] J. Qi, N. Edirisinghe, M.G. Rabbani, M.P. Anantram, Phys. Rev. B 87 (2013) 085404.
[32] Y. Li, J.M. Artes, J. Qi, I.A. Morelan, P. Feldstein, M.P. Anantram, J. Hihath, J. Phys. Chem. Lett. 7 (2016) 1888–1894.
[33] E. Beall, S. Ulku, C. Liu, E. Wierzbinski, Y. Zhang, Y. Bae, P. Zhang, C. Achim, D.N. Beratan, D.H. Waldeck, J. Am. Chem. Soc. 139 (2017) 6726–6735.
[34] M. Kilgour, D. Segal, J. Chem. Phys. 143 (2015) 024111.
[35] M. Kilgour, D. Segal, J. Phys. Chem. C 119 (2015) 25291–25297.
[36] M. Kilgour, D. Segal, J. Chem. Phys. 144 (2016) 124107.
[37] H. Kim, M. Kilgour, D. Segal, J. Phys. Chem. C 120 (2016) 23951–23962.
[38] R. Korol, M. Kilgour, D. Segal, J. Chem. Phys. 145 (2016) 224702.
[39] H. Kim, D. Segal, J. Chem. Phys. 146 (2017) 164702.
[40] J.C. Klöckner, R. Siebler, J.C. Cuevas, F. Pauly, Phys. Rev. B 95 (2017) 245404.
[41] S. Datta, TLAB Scripts for Quantum Transport: Atom to Transistor, 2005, https://nanohub.org/resources/103.
[42] C.W. Groth, M. Wimmer, A.R. Akhmerov, X. Waintal, New J. Phys. 16 (2014) 063065.
[43] J.E. Fonseca, T. Kubis, M. Povolotskyi, B. Novakovic, A. Ajoy, G. Hegde, H. Ilatikhameneh, Z. Jiang, P. Sengupta, Y. Tan, G. Klimeck, J. Comput. Electron. 12 (2013) 592.
[44] S. Birner, T. Zibold, T. Andlauer, T. Kubis, M. Sabathil, A. Trellakis, P. Vogl, IEEE Trans. Electron Devices 54 (2007) 2137.
[45] M. Brandbyge, J.-L. Mozos, P. Ordejon, J. Taylor, K. Stokbro, Phys. Rev. B 65 (2002) 165401.
[46] N. Papior, N. Lorente, T. Frederiksen, A. García, M. Brandbyge, Comput. Phys. Comm. 212 (2017) 8–24.
[47] A.R. Rocha, V.M. García Suarez, S. Bailey, C. Lambert, J. Ferrer, S. Sanvito, Phys. Rev. B 73 (2006) 085414.
[48] M. Di Ventra, Electrical Transport in Nanoscale Systems, Cambridge University Press, Cambridge, U.K, 2008.
[49] S. Bedkihal, M. Bandyopadhyay, D. Segal, Eur. Phys. J. B 86 (2013) 506.
[50] G. Benenti, G. Casati, K. Saito, R.S. Whitney, Phys. Rep. 694 (2017) 1.
[51] DNA molecules are connected to the leads in the 3' ends, in accord with experiments [14,15] and numerical simulations [37–39]. The sketch in Ref. [38] erroneously displays the meal leads at the 5' ends.
[52] K. Senthilkumar, F.C. Grozema, C.F. Guerra, F.M. Bickelhaupt, F.D. Lewis, Y.A. Berlin, M.A. Ratner, L.D.A. Siebbeles, J. Am. Chem. Soc. 127 (2005) 14894–14903.
[53] M. Zilly, O. Ujsaghy, D.E. Wolf, Phys. Rev. B 82 (2010) 125125.
[54] Y. Zhang, C. Liu, A. Balaeff, S.S. Skourtis, D.N. Beratan, Proc. Natl. Acad. Sci. 111 (2014) 10049–10054.
[55] P. Woiczikowski, T. Kubar, R. Gutierrez, R. Caetano, G. Cuniberti, M. Elstner, J. Chem. Phys. 130 (2009) 215104.
[56] T. Hansen, G. Solomon, J. Phys. Chem. C 120 (2016) 6295–6301.
[57] P. Sam-ang, M. Reuter, New J. Phys. 19 (2017) 053002.
[58] D. Nozaki, C. Toher, J. Phys. Chem. C (2017). http://dx.doi.org/10.1021/acs.jpcc.6b11951.
[59] C. Seth, V. Kaliginedi, S. Suravarapu, D. Reber, W. Hong, T. Wandlowski, F. Lafolet, P. Broekmann, G. Royal, R. Venkatramani, Chem. Sci. 8 (2017) 1576–1591.
[60] C. Guo, K. Wang, E. Zerah-Harush, J. Hamill, B. Wang, Y. Dubi, B. Xu, Nature Chem. 8 (2016) 484–490.